Journal of
MATERIALS RESEARCH

Surface microstructure of $Zr_{41.25}Ti_{13.75}Cu_{12.5}Ni_{10.0}Be_{22.5}$, a bulk metallic glass

M. A. LaMadrid
Division of Engineering and Applied Science, California Institute of Technology, Pasadena, California 91109

S. D. O'Connor
Division of Chemistry and Chemical Engineering, California Institute of Technology, Pasadena, California 91109

A. Peker and W. L. Johnson
Division of Engineering and Applied Science, California Institute of Technology, Pasadena, California 91109

J. D. Baldeschwieler
Division of Chemistry and Chemical Engineering, California Institute of Technology, Pasadena, California 91109

(Received 16 June 1995; accepted 14 February 1996)

The surface of $Zr_{41.25}Ti_{13.75}Cu_{12.5}Ni_{10.0}Be_{22.5}$, a bulk metallic glass prepared by RF induction melting, has been imaged using atomic force microscopy. The untreated surfaces were very smooth; features were no higher than 3 nm over a 10×10 μm region, comparable to many polished surfaces. Two types of microstructure were also observed; periodic striations forming either a striped or a checkered structure were present, with wavelengths between 1 and 2 μm, and amplitude of approximately 2 nm; in other cases, "cracked mud"-like patterns were observed. These microstructures could be related to strain-induced surface roughening; preliminary calculations are presented that are consistent with this hypothesis.

I. INTRODUCTION

Recently, Peker and Johnson discovered a class of easily processible metallic glasses.[1] These glasses require cooling rates of 10 K/s or less, orders of magnitude slower than traditional metallic glasses, and can be heated well above the glass transition temperature without crystallization. Metallic glasses possess many technologically useful properties, including high strength/weight ratio, high wear resistance, low frictional coefficient, and high corrosion resistance. Previous metallic glasses require cooling rates of 10^6 K/s or more, producing only thin films or foils, limiting their application. These other types of glasses also crystallize below the glass transition temperature (T_g). These new metallic glasses can be manufactured with dimensions thicker than an inch and processed above T_g. These properties increase substantially the usefulness of metallic glasses.

The correlation among surface topography, surface chemistry, and friction in these metallic glasses is under investigation in our laboratory. This report presents the topographic results obtained using atomic force microscopy. Three types of surface structures have been observed: (i) Disordered regions with roughness smaller than 3 nm. (ii) Periodic stripes and checkered patterns with wavelengths between 1 and 3 μm and amplitudes between 2 and 3 nm. (iii) Regions that appear as cracked mud-like patterns.

II. EXPERIMENTAL DETAILS

The samples were bulk metallic glass (BMG) ingots of $Zr_{41.25}Ti_{13.75}Cu_{12.5}Ni_{10.0}Be_{22.5}$, ranging in size from 2–10 mm in diameter. They were prepared by induction melting on a water-cooled silver boat under a titanium gettered argon atmosphere. X-ray diffraction showed broad peaks characteristic of amorphous materials. High resolution TEM on similar samples showed no ordered features larger than 1.2 nm. X-ray photoemission spectroscopy studies have shown the presence of an oxide surface composed of Zr, Ti, and Be.[2] The samples looked very shiny and smooth to the naked eye. The smaller samples were mounted on steel washers with 5-min epoxy. Larger samples were first sectioned with a diamond saw in oil, washed in an ultrasonic cleaner (acetone/methanol/deionized water sequence), then mounted as before.

Atomic force microscopy (AFM) has been used as a very sensitive tool for imaging flat surfaces, even on an atomic scale.[3,4] To image using AFM, a cantilever with a small pyramidal tip is placed over the sample and

lowered into mechanical contact. A tube piezoceramic is then used to scan the tip over the sample. The deflection of the cantilever corresponds to changes in height of the sample. These motions are monitored by reflecting a laser beam from the cantilever and onto a position sensitive photodiode. The lateral or frictional force can also be determined by using a four-quadrant detector.[5]

A Topometrix AFM system with in-house software was used in contact mode for all of these experiments.[6,7] All of the images were taken in air with standard pyramidal tips (Si_3N_4); two scanners were used, a 10 μm tube scanner and a 75 μm pivoting scanner. The samples imaged were unusual for AFM due to their relatively small radius of curvature. All of the samples studied in this report were at least 2 mm high; metal spacers were used to lower the scanning stage to accommodate the large sample height. The Topometrix instrument was equipped with a video camera that images the tip-sample interface at a 45° angle. It was straightforward to position the tip at the top of the spherical samples by noting the reflection of the light off the sample as it was translated. Prior to imaging, all of the samples were rinsed with acetone/methanol/de-ionized water, then blown dry with pressurized air to remove excess surface contaminants.

A total of nine BMG samples prepared by RF (radio frequency) levitation melting were studied. For comparison, a crystalline sample of different composition and a sample made by electrostatic levitation were also imaged. The results presented are from three of the RF levitated samples. Sample I was the top region of a large ingot (~10 mm in diameter) that had been sectioned. Sample II was a small spherical ingot (~3.5 mm in diameter). Sample III was also spherical (~2.5 mm in diameter). All of the images presented were acquired at a scan rate of 4 lines/second and 250 pixels/line, although the scanning rate was varied to check for imaging artifacts. We also zoomed in on features, changed the scanning direction, and rotated some of the samples to verify that the observed features were reproducible. The contact force in these experiments was 20–50 nN and caused no noticeable wear; the images were very reproducible over many consecutive scans.

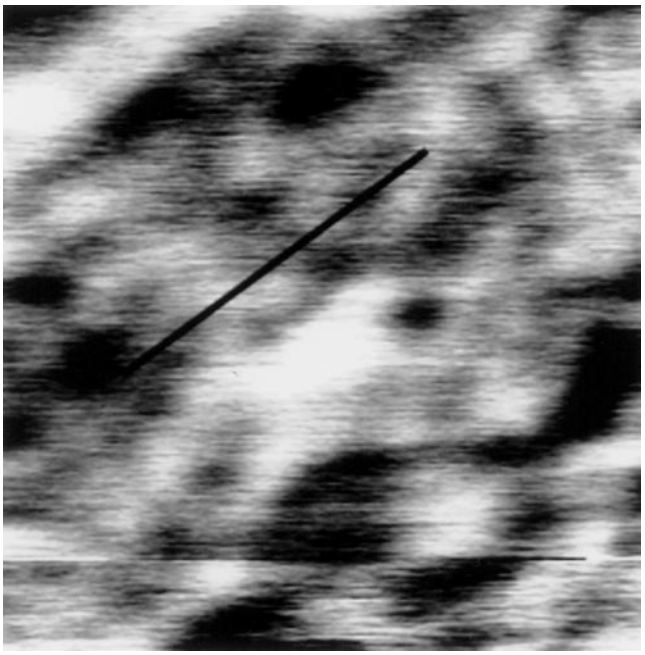

(a)

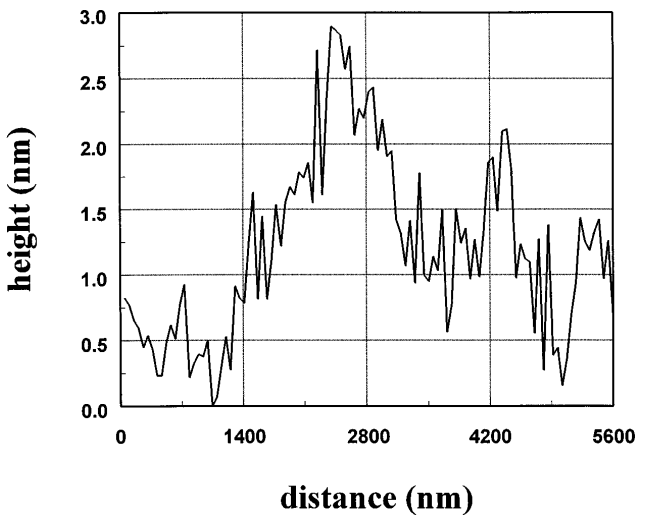

(b)

FIG. 1. (a) A 10 × 10 μm AFM image of sample I; the data have been line leveled only. This area is relatively flat with no repeating features. (b) AFM linecut; the plot represents the quantitative height data along the line drawn in (a). Even the large feature just below the linecut is only 2 nm high.

III. RESULTS

Figure 1(a) is an image of the top surface of sample I. As seen in the linecut [Fig. 1(b)], the surface features are less than 3 nm over the 10 × 10 μm region. No repeating patterns are present. The surface is remarkably flat, even though no polishing was performed. Figure 2(a) is a 10 × 10 μm image of sample II. The figure shows an unexpected striped pattern. These stripes have wavelengths slightly less than 2 μm and amplitudes ranging from 2–3 nm [see Fig. 2(b)]. In some regions, smaller wavelengths are also observed [Fig. 3(a)], as well as cross-hatched structures [Fig. 3(b)]. Figure 4 is a 50 × 50 μm image of sample III. The wavelength and direction of the corrugations are variable over this distance. The other features are probably surface contaminants.

Figure 5 is a 4.5 × 4.5 μm image of sample II. Notice the cracked mud-like pattern that is present, as well as the small aggregates (~100 nm in diameter) that are formed. The surface roughness is much larger (~10 nm)

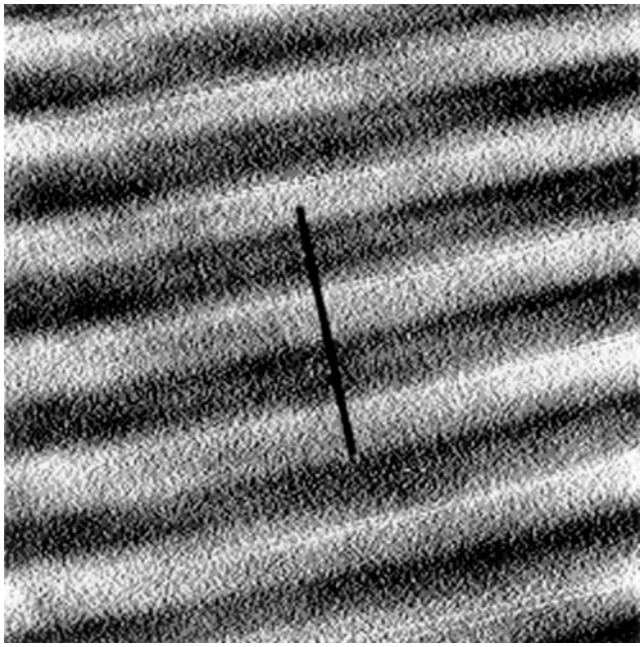

(a)

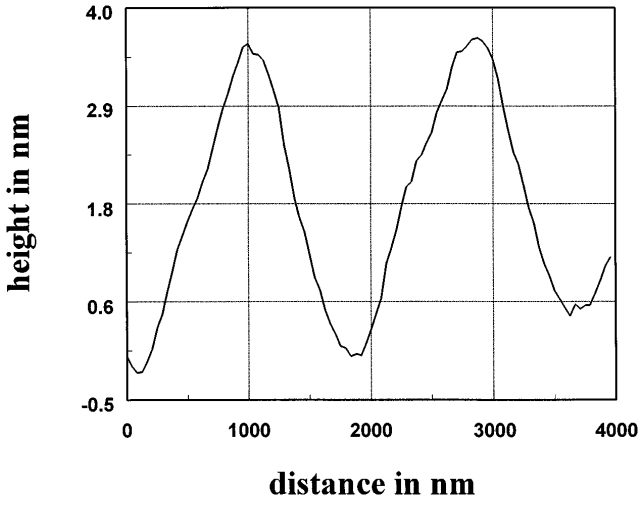

(b)

FIG. 2. (a) A 10×10 μm AFM image of sample II; notice the periodic corrugation. (b) The linecut shows that the wavelength of the corrugation is ~ 2 μm with an amplitude ranging between 2 and 3 nm.

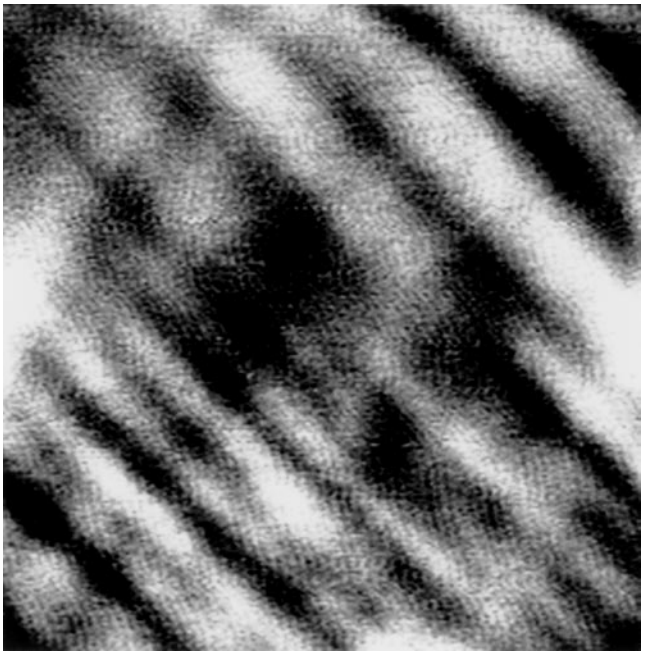

(a)

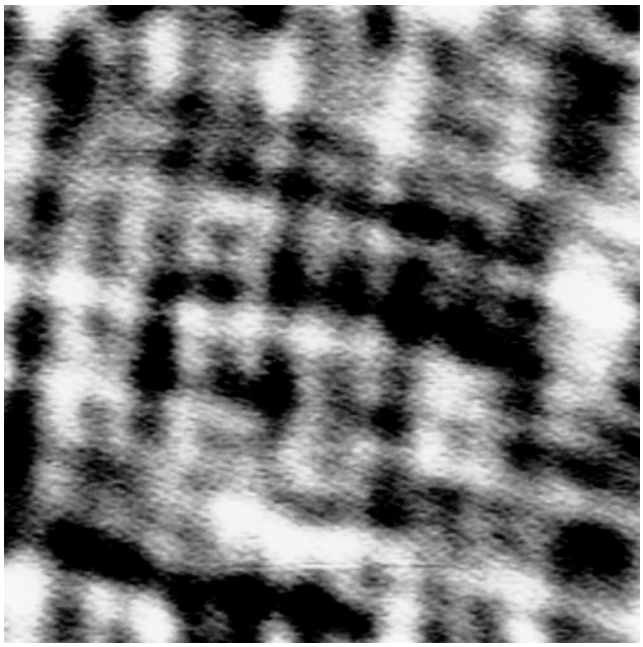

(b)

FIG. 3. (a) A 10×10 μm AFM image of a different area of sample II; two wavelengths are present, with one roughly half the size of the other. (b) A 10×10 μm AFM image of sample II showing a cross-hatched pattern; the wavelength is ~ 0.8 μm.

when these features are observed. The "cracks" are not appreciably deeper than the other features; however, they do seem to form repeating patterns as observed in the figure.

Some type of periodic corrugation was present in six of the nine samples; the cracked-mud-like patterns were observed in eight out of nine samples. Since only the top portion of the samples could be imaged, it is difficult to elucidate how extensively these features cover the sample surface with this technique. The periodic structures were present only in the small samples—the largest sample did not show any periodicities. Also, the partially crystallized sample and the electrostatically levitated sample (which was cooled more slowly than the induction melted samples) did not show any regular corrugations.

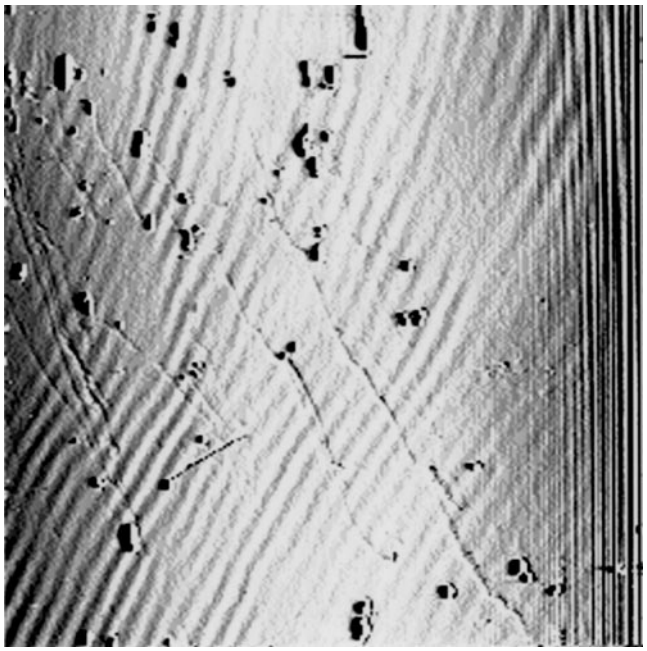

FIG. 4. A 50 × 50 μm AFM image of sample III. The wavelength and direction shift slightly over this large area. The bright spots are probably surface contaminants.

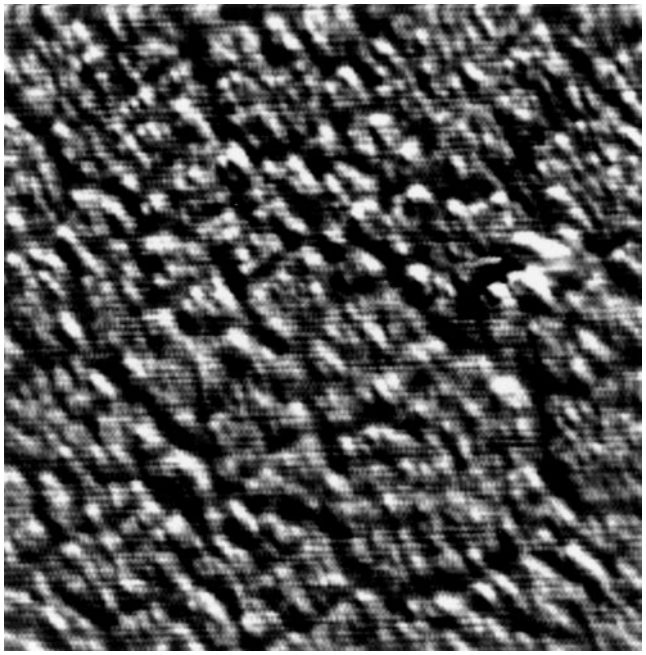

FIG. 5. A 4.4 × 4.4 μm region of sample II; a cracked mud-like pattern is present in this region.

IV. DISCUSSION

All of the samples prepared for this report showed remarkably smooth surfaces. No polishing or "high-tech" preparation was required to produce surfaces with only nm roughness over 10 μm regions. However, the surfaces did exhibit very interesting structure on the nm scale. Most interesting is the periodic corrugations that were observed in six of the samples. We hypothesize that the stripes could arise from the relief of the strain.

Using continuum mechanics, it has been shown that when an elastic body with a flat surface is nonhydrostatically (uniaxially or biaxially) stressed, the surface may be unstable.[8–16] Undulations may grow with wavelengths that are governed by the competition between stress relaxation and surface tension or gravity. This surface instability has been referred to as strain-induced surface roughening or the Grinfeld instability. The most unstable wavelength (i.e., the wavelength that should be observed) will depend on the mechanism of surface mobility, for example, diffusion or evaporation/condensation.

Linear stability analysis defines a critical wavelength by[9,12]

$$\lambda > \lambda_0 = \pi\gamma/M\sigma^2,$$

where γ is the surface tension and σ is the applied stress. The factor M depends on the boundary condition; for plane stress, $M = 1/E$; for plane strain, $M = (1 - \nu^2)/E$, where E is Young's modulus and ν is Poisson's ratio. It is unclear whether the applied stress arises from plane strain, plain stress, or from some combination of the two. Therefore, both situations are considered.

The dominant mass transport mechanism will determine the maximally unstable wavelength, λ_m. For transport by surface diffusion, $\lambda_m(4/3)\lambda_0$; for evaporation/condensation, $\lambda_m = 2\lambda_0$. It is problematic to calculate the exact value for λ_m in this system. However, an order-of-magnitude calculation is instructive.

In order to solve for σ, the following approximations are used: $E = 93$ GPa, $\nu = 0.3$,[17] and $\gamma = 1.0$ J/m^2 [18]; $\lambda_m = 1.5$ μm is the observed wavelength. A stress (σ) of 0.5–0.6 GPa is needed to create the observed instability, depending on whether the plane strain or plane stress boundary conditions are used. A stress of 0.5 GPa corresponds to ~0.5% strain at room temperature for this alloy.[17]

Most of the nonhydrostatic stress in these samples should be due to thermal stress. The sample is cooled mainly by contact with the silver holder, causing a temperature gradient from the top to the bottom. In addition, the surface of the sample cools before the interior. Assuming that the mass transport at the surface is significant only near and above the glass transition temperature (T_g = 350 °C), and the sample cools through a ΔT of 300–500 °C (i.e., the initial temperature is between 650 and 850 °C; the final temperature is ~350 °C), a coefficient of thermal expansion of $1.0–1.7 \times 10^{-5}$/°C produces a 0.5% strain. Preliminary measurements indicate that the coefficient of thermal expansion at T_g is approximately 9×10^{-4}/°C below and 2×10^{-5}/°C above T_g.[19] Young's modulus, Poisson's ratio, and surface tension are not yet rigorously

known for this material near T_g, but the values used in this calculation should be within a factor of 2 of the true values.

Assuming surface diffusion to be the dominant mass transport mechanism, a diffusion constant of 10^{-13}–10^{-14} m^2/s is required for atoms to travel a few μm in ~10 s. The bulk diffusion constant for Be is 10^{-18} m^2/s near T_g for this alloy.[20] In crystals, surface and grain boundary self-diffusion constants are 6–8 orders of magnitude larger than in the bulk near the melting temperature (T_m). Typically, $T_g = 0.6$–$0.7\ T_m$ for good glass formers.[21] Therefore, it is quite plausible that the surface diffusion constant is large enough for the instability to occur near T_g.

Similar corrugations were observed in solid He as it was quenched over a few millidegrees,[22] although the wavelength observed (mm's) corresponded to the low stress limit of the instability, in which gravity was the dominant opposing factor. Interestingly, the corrugations in helium disappeared once the temperature was restabilized.[23] Further studies using piezoelectric transducers confirmed that the corrugations were stress induced.[23] Thin films of InGaAs on GaAs[24] and Si/Ge,[16,25,26] where lattice mismatch causes stresses of a few GPa, have also exhibited the Grinfeld instability. Crack-like corrugations were observed in a crystallized polymer, and the authors speculated that the stress was due to the preferential orientation of the crystallization.[27]

Since surface diffusion in these materials has not yet been measured, this hypothesis is still speculative and requires further systematic measurements of both the surface diffusion constant and the dependence of the wavelengths observed on various parameters. The fact that periodic structures were not seen in the largest samples is consistent with our model, since the slower cooling rate would induce a much smaller stress. If it is assumed that radiative cooling dominates at the top of the samples, the larger samples would exhibit cooling rates an order of magnitude slower than the small samples. Since the wavelength are proportional to the inverse square of the stress, and the stress is directly proportional to the cooling rate, the larger samples should exhibit wavelengths that are ~2 orders of magnitude longer than the small samples. These large periodic structures would not be observed in our AFM system. Similarly, the electrostatic levitated samples, which were 2 mm in diameter but cooled at approximately 1–2 K/s, did not show any regular corrugations. The actual cooling rate will depend not only on radiative cooling, but also conduction and convection.

It is possible that the stress is due to a mismatch between the oxide layer and the bulk, in addition to thermal stress. This issue can be addressed by synthesizing samples in UHV and imaging *in situ*, with a controlled introduction of oxygen. In addition, calculations suggest that variations in composition may induce stress which can affect the stability of film growth.[28] It is unclear how these calculations can be applied to amorphous systems, but XPS results show a surface oxide layer composed of Zr, Ti, and Be, which is different than the bulk composition.[2] Sputter depth profiling was not performed.

It is also not clear how the observed half-wavelengths and cross hatching can be accounted for by the current models, other than that the stress is probably not truly uniaxial and could contain multiple vector components. In addition, we have not yet determined what causes the preferred orientation of the stripes. Since only a very limited region of the samples could be imaged, it is difficult to speculate on the preferred orientation of the stripes in other areas of the sample. Also, it has not been determined how the orientation of these structures depends on the direction of the temperature gradient.

A few other possible causes for the periodic corrugations were explored and found to be inconsistent with observations:

(1) X-ray microprobe analysis of these samples failed to detect any variations in the composition of Zr, Ti, Cu, or Ni within the resolution of the instrument (2%). This result seems to eliminate the possibility that local chemical differences cause the corrugations.

(2) Samples were synthesized while vibrating the RF levitation container at 60 Hz (as well as its harmonics); no correlation was found between the vibration frequency and the presence of the periodic corrugations.

(3) The capillary and gravity wavelengths for this material are at least a few millimeters, well above the observed wavelengths.

(4) The periodic corrugations resemble interference fringes; the AFM uses an optical beam alignment to detect small cantilever deflections. However, it is difficult to see how the experimental geometry could produce corrugations similar to those observed. In addition, these fringes would be present in all shiny, curved samples imaged, since stray reflections are hard to avoid. The periodic corrugations appeared only in some samples.

It is unclear at present what causes the crack-like mud patterns. They may be related to the oxidation process, since these structures were more prevalent in samples that were imaged a few months after synthesis. There have been suggestions that Grinfeld instability is a precursor to crack formation.[12,29] If this observation is correct, then the cracked-mud-like patterns in these samples could be a manifestation or a more evolved version of the instability. However, these patterns have been observed in both fresh samples and older samples (a few months), as well as coexisting with the periodic ripples. Clearly, more systematic studies are required.

V. CONCLUSION

The surfaces of the bulk metallic glass $Zr_{41.25}Ti_{13.75}Cu_{12.5}Ni_{10.0}Be_{22.5}$ have been imaged with AFM. The surfaces are remarkably flat, with surface features no higher than 3 nm over a 10 μm region. In some cases, surprising periodic corrugations and cracked-mud-like patterns were observed. A plausible source for these features is strain-induced surface roughening or Grinfeld instability due to the relief of nonhydrostatic thermal stress.

ACKNOWLEDGMENTS

M. A. LaMadrid was supported by a NRC Ford Foundation fellowship, an AAUW fellowship, and by a grant from the Department of Energy (DEFG0386 ER45242). S. D. O'Connor was supported by an NIH training grant. We thank Y. J. Kim for providing us with the electrostatically levitated samples, and X. H. Lin for the crystallized sample. The authors would also like to acknowledge useful conversations with M. Cross, B. Spencer, and D. Meiron.

REFERENCES

1. A. Peker and W. L. Johnson, Appl. Phys. Lett. **63**, 2342 (1993).
2. M. A. LaMadrid, A. Peker, R. Housley, A. Rice, and W. L. Johnson, unpublished.
3. G. Binnig, C. F. Quate, and C. Gerber, Phys. Rev. Lett. **56**, 930 (1986).
4. T. R. Albrecht and C. F. Quate, J. Appl. Phys. **62**, 2599 (1987).
5. G. Meyer and N. M. Amer, Appl. Phys. Lett. **57**, 2089 (1990).
6. Topometrix, Santa Clara, CA.
7. D. R. Baselt, S. M. Clark, M. G. Youngquist, C. F. Spence, and J. D. Baldeschwieler, Rev. Sci. Instrum. **64**, 1874 (1993).
8. R. J. Asaro and W. A. Tiller, Metall. Trans. **3**, 1789 (1972).
9. D. J. Srolovitz, Acta. Metall. **37**, 621 (1989).
10. P. Nozieres, J. Phys. I **3**, 681 (1993).
11. M. A. Grinfeld, Sov. Phys. Dokl. **31**, 831 (1987).
12. W. H. Yang and D. J. Srolovitz, Phys. Rev. Lett. **71**, 1593 (1993).
13. B. J. Spencer, P. W. Voorhees, and S. H. Davis, Phys. Rev. Lett. **67**, 3696 (1991).
14. L. B. Freund and F. Jonsdottir, J. Mech. Phys. Solids **41**, 1245 (1993).
15. H. J. Gao, J. Mech. Phys. **39**, 443 (1991).
16. J. Tersoff and F. K. LeGoues, Phys. Rev. Lett. **72**, 3570 (1994).
17. H. A. Bruck, T. Christman, A. J. Rosakis, and W. L. Johnson, Scripta Metall. Mater. **30**, 429 (1994).
18. The surface tensions of the component metals range from $1-2$ J/m^2 at their respective melting points; E. Brandes and G. Brook, *Smithells Metals Reference Book* (1992).
19. E. Bakke and W. L. Johnson, private communication.
20. U. Geyer, S. Schneider, W. L. Johnson, and T. Tombrello, unpublished.
21. W. L. Johnson, in *Intermetallic Compounds*, edited by J. H. Westbrook and R. L. Fleischer (John Wiley and Sons Ltd., New York, 1994), Chap. 29.
22. J. Bodensohn, K. Nicolai, and P. Leiderer, Z. Phys. B **64**, 55 (1986).
23. R. H. Torii and S. Balibar, J. Low-Temp. Phys. **89**, 391 (1992).
24. J. A. Venables, G. D. T. Spiller, and M. Hanbucken, Rep. Prog. Phys. **47**, 399 (1984).
25. D. E. Jesson, S. J. Pennycook, J. M. Baribeau, and D. C. Houghton, Phys. Rev. Lett. **71**, 1744 (1993).
26. A. G. Cullis, D. J. Robbins, A. J. Pidduck, and P. W. Smith, J. Cryst. Growth **123**, 333 (1992).
27. J. Berrehar, C. Caroli, C. Lapersonne-Meyer, and M. Schott, Phys. Rev. B **46**, 13 487 (1992).
28. J. E. Guyer and P. W. Voorhees, Phys. Rev. Lett. **74**, 4031 (1995).
29. B. J. Spencer and D. J. Meiron, Acta Metall. Mater. **42**, 3629 (1994).